LOW-FREQEUNCY NOISE IN III-V NITRIDE 2D ELECTRON AND HOLE GASES

Nima Leclerc[1*], Menyoung Lee[2], Reet Chaudhuri[2], Huili Grace Xing[1,2] & Debdeep Jena[1,2]

Following the use of the Mg-doped GaN for p-channel transistor channels, the manipulation of holes and their interactions with phonons, impurities, and dislocations remains a fundamental challenge. *p*-channel GaN electronics have received recent interest due to the relatively high hole mobility in AlN-GaN polarization induced two-dimensional hole gases (2DHGs). Although the mobility-limiting scattering mechanisms in 2DHGs is understood, the origins of 1/*f* noise in these channels is not. We introduce a characterization technique and stochastic model to identify 1/*f* noise mechanisms in a two-dimensional electron gas which can be extended to the 2DHG.

The origins of low-frequency or 1/*f* noise has remained a controversial topic since it was first discovered in vacuum tubes in the 1950s[1,2]. 1/*f* noise refers to the phenomena where the noise power spectral density $S_x(f)$ with state x for a stochastic process has the form $S_x(f) \propto 1/f^{\alpha}$ with α as a constant. The current (voltage) power spectral density $S_I(f)$ ($S_V(f)$) in semiconductor channels will typically have a 1/*f* frequency dependence below 1 MHz and remain constant above this cutoff frequency.

Two models provided by Hooge[3,4] and McWorther[5,6] have been relied upon for decades in identifying the origin of 1/*f* noise in semiconductor materials and devices. Hooge attributes the current noise δI to mobility fluctuations and defines $S_I(f)$ as shown in Equation 1.

$$\frac{S_I}{I^2} = \frac{S_\mu}{\mu^2} = \frac{\alpha_H}{Nf} \qquad (1)$$

Above μ is the carrier mobility, N is the number of carriers, and α_H is the material dependent noise parameter and extensive experimental work has been carried out to validate Hooge's claims about mobility fluctuations mediating noise across materials from Si to graphene[7,8,9]. McWorther attributes 1/*f* noise to number fluctuations and this has been observed in GaN-AlGaN two-dimensional electron gases (2DEGs) due to generation-recombination events[10,11,12]. In this work, we extend measurements[13,14,15] and Hooge's noise models to identify the origins of this phenomena in AlGaN/GaN 2DEGs and two-dimensional hole gases (2DHGs)[16,17].

Characterizing 1/*f* noise at III-V interfaces

Understanding the influence of voltage bias on the voltage noise spectrum $S_V(f)$ of a transistor is critical in optimizing the signal-to-noise ratio (SNR) for high-speed communication device applications[18,19,20]. We consider the bias and frequency dependences of S_V in AlGaN-GaN high electron mobility transistors (HEMTs) with a polarization-induced 2DEG channel fabricated in our group[21]. As depicted in the device schematic in Figure 1(b), the transistor comprises a stack of GaN-AlGaN-AlN layers and the 2DEG channel lies at the AlGaN/GaN interface. A bias V_{DS} is applied across the source-drain channel, allowing current to flow across the 2DEG where the current I_{DS} encounters fluctuations from generation-recombination events, polar optical phonon scattering, acoustic phonon scattering, and dislocation scattering. The applied gate voltage V_{GS} modulates the 2DEG sheet density n_s[21] and leads to number density fluctuations in the noise current expression: $\delta I_{DS}(t) \propto n_s\, \delta\mu + \mu\, \delta n_s$. We perform bias-

[1]Department of Materials Science and Engineering, Cornell University, Ithaca, New York 14853, USA.
[2]School of Electrical and Computer Engineering, Cornell University, Ithaca, New York 14853, USA.

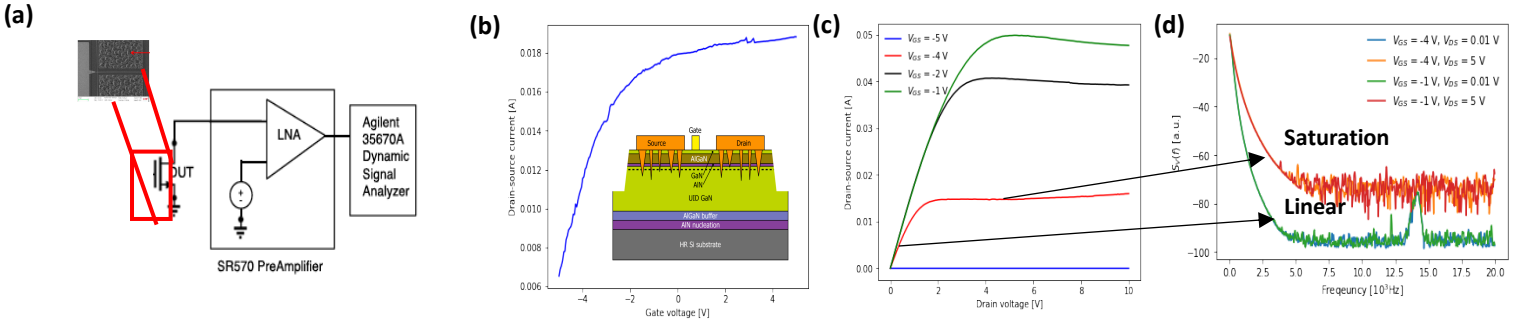

Figure 1: (a) *1/f noise measurement setup for a 3 -terminal transistor. Device is biased at V_{DS}/ V_{GS} and the channel current passes through an SR570 LNA and is then measured by a noise spectrum analyzer.* ***(b)*** *$I_{DS} - V_{GS}$ of the AlGaN-GaN channel HEMT at $V_{DS} = 5$ V illustrating good turn-on characteristics. Dashed line in the HEMT schematic depicts the 2DEG channel at the AlGaN-GaN interface.* ***(c)*** *$I_{DS} - V_{DS}$ characteristic illustrates good turn-on behavior with varied V_{GS}.* ***(d)*** *Voltage noise spectra collected from room-temperature measurements demonstrating 1/f behavior in linear and saturation regimes.*

dependent S_V measurements to understand the interplay between the 2DEG sheet carrier density n_s and S_V. We performed room temperature S_V measurements under different V_{DS} and V_{GS} bias conditions in an AlGaN-GaN HEMT with a gate length $L_{DS} = 12\ \mu$m and source-drain length $L_{DS} = 1\ \mu$m. Following the circuit diagram in Fig. 1(a), the device is biased with V_{DS} and V_{GS} allowing a current $I_{DS} = I_{DS,0} + \delta I_{DS}(t)$ to flow across the 2DEG. I_{DS} is fed into a series of low-pass filters ($f_c = 1$ MHz) which outputs only the low-frequency components of $\delta I_{DS}(t)$ into a low-noise amplifier (LNA), and an Agilent 35670A Dynamic Signal Analyzer is used to measure $S_V(f)$.

The voltage noise spectra are collected in the linear (saturation) regimes of the HEMT corresponding to $V_{DS} = 0.01\ V$ (5 V) for a range of gate biases V_{GS} (Fig. 1(b,c,d)). The noise spectra demonstrate the expected $1/f$ behavior below ~ 5 kHz for all bias conditions indicating that either mobility or carrier number fluctuations are present in the channel (Fig. 1(d)). We observe that that the noise power $S_V(f)$ increases quadratically with V_{DS} as expected from its definition. This implies that $S_V(f)$ is small prior to channel inversion and becomes field-dominated once the channel is saturated which agrees with prior noise studies of AlGaN-GaN HEMTs[22,23]. The $S_V(f)$ profiles show little variation with V_{GS}, which implies that the channel noise current $\delta I_{DS}(t)$ is not sensitive to carrier number fluctuations and that the $\mu\ \delta n_s$ contribution is negligible. However, this is in disagreement with previous measurements performed on similar devices. We suspect that this disagreement with previous findings is due to the high noise floor of the spectrum analyzer combined with the noise added by the voltage bias source. Significant efforts are necessary to minimize external noise contributions below the noise floor of the transport channel. Our measurements do not capture the effects that channel mobility fluctuations have on the noise spectrum because of the high noise floor and the requirement of temperature-dependent $S_V(f)$ measurements.

Modeling *1/f* noise in GaN/AlN heterostructures from mobility fluctuations

Temperature, frequency, and bias dependence of $S_I(f)$ provides additional information about the microscopic origins of $1/f$ noise. We developed a simple stochastic transport model that relates mobility fluctuation events due to electron-phonon scattering in the channel to the current autocorrelation function $C_I(\tau)$. The Monte Carlo simulator extends previous work in predicting the phonon-limited high-field transport in FETs[24,25,26,27]. Our implementation is critical in predicting the $1/f$ noise spectra of devices because it tracks the stochastic evolution of electron (hole) occupation over k-states in the Brillouin zone under the influence of an external field and mobility-limiting scattering events[28,29]. Importantly, our algorithm accounts for two processes present in electron (hole) transport: drift and diffusion. The equilibrium band structure of the 2DEG (2DHG), timestep δt, simulation time T_{sim}, external field **E**, scattering events

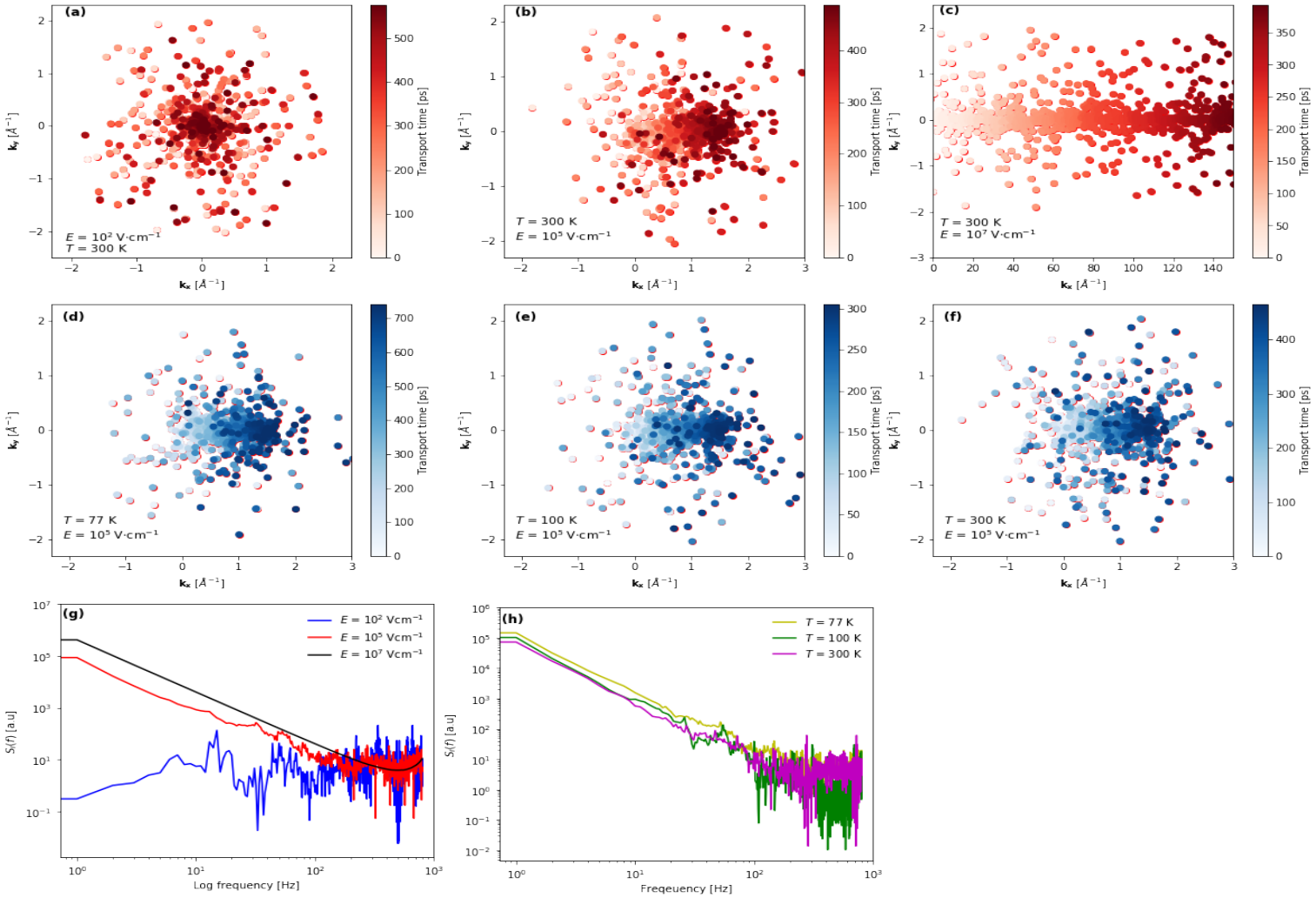

Figure 2: ***(a)*** *k-state evolution due to APs/POPs with a field strength of 100 V/cm at 300 K shows that scattering (diffusion) dominates electron transport.* ***(b)*** *k-state evolution with a field strength of 10^5 V/cm at 300 K.* ***(c)*** *k-state evolution due to APs/POPs with a field strength of 10^5 V/cm at 300 K shows that field (drift) dominates electron transport.* ***(d)*** *k-state evolution with a field strength of 10^5 V/cm at 77 K* ***(e)*** *k-state evolution with a field strength of 10^5 V/cm at 100 K* ***(f)*** *k-state evolution with a field strength of 10^5 V/cm at 300 K.* ***(g)*** *Simulated noise power density of 2DEG at 300 K with varied field strength over frequencies in log-log scale shows clear 1/f trend and power law scaling.* ***(h)*** *Simulated noise power density of 2DEG at 10^5 V/cm with varied temperature over frequencies in log-log scale shows expected trend that noise amplitude increases at low T.*

(e.g. acoustic phonons), and material parameters quantifying the scattering rates (e.g. acoustic deformation potential) are specified according to the desired simulation constraints. Once the simulation begins, the electrons in states $|\mathbf{k}_i>$ deterministically drift to unoccupied states $|\mathbf{k}_{i+1}>$ according to the evolution $\mathbf{k}_{i+1} = \mathbf{k}_i + \frac{e\,\mathbf{E}}{\hbar}\delta t$ from Newton's equations. The electron then stochastically diffuses to an unoccupied state $|\tilde{\mathbf{k}}_i>$ according to a probability distribution $\mathcal{P}(\mathbf{k}_{i+1} \mid \mathbf{k}_i)$. Determining $\mathcal{P}(\mathbf{k}_{i+1} \mid \mathbf{k}_i)$ is essential in capturing the noise physics of the channel because it depends on the electron (hole) scattering rates $\tau^{-1}{}_{\mathbf{k}_{i+1},\mathbf{k}_i}$ due to collisions with intrinsic and extrinsic scatterers. These scattering rates depend on measurable experimental parameters like temperature and the material's band structure. In modeling the noise spectrum for the AlGaN/AlN 2DEG (2DHG) we consider only intraband polar optical phonon (POP) and acoustic phonon (AP) scattering events using Fermi's golden rule[30] to determine scattering rates. The *k*-states occupied over the simulation are tracked over ~100 ps determining the current autocorrelation function $C_I(\tau)$. The noise power spectral density $S_I(f)$ (the Fourier transform of $C_I(\tau)$) is used to predict the temperature, frequency, and field dependence of the $1/f$ noise. Further implementation details can be found in the Extended Methods section.

Temperature-dependent mobility measurements of 2DEGs(2DHGs) suggest that the high-temperature mobility of these channels is limited by POP/AP scattering mechanisms making it

reasonable to assume that these are dominant 1/*f* noise mechanisms and can be exclusively used in our model. We simulate the temperature and bias dependent noise spectra for the AlGaN/GaN electron channel influenced by both POP and AP with a parabolic band structure ($E \sim k^2$) and material parameters obtained from the literature[31]. We set the drift timestep to 1 fs (~1,000 shorter than the diffusion time) and track the *k*-state evolution over ~500 ps with 10,000 *k*-points. Figure 2(a, b, c) shows how this evolution changes under the influence of 10^2, 10^5, and 10^7 Vcm^{-1} electric fields corresponding to the linear and saturation operating regimes. When field is driven from 10^2 Vcm^{-1} up to 10^7 Vcm^{-1} (Fig. 2(b,c)), the electron transport is strongly influenced by drift as electrons are encouraged to fill unoccupied states in the direction of the field over time. This implies that at higher fields (in the saturation regime), the low-frequency SNR is not sensitive to mobility fluctuations. The noise spectrum $S_I(f)$ at each bias is plotted in Fig. 3(g) and demonstrates the expected $1/f$ behavior at high biases and remains flat at low bias, which is sensible given that little current flows through the channel under very low field strengths. The noise spectra at high fields (10^2 Vcm^{-1} and 10^7 Vcm^{-1}) demonstrate the expected power law trend with applied field.

The temperature-dependence of $S_I(f)$ is critical in identifying the origins of mobility fluctuations leading 1/*f* noise. Since $S_I(f) \propto \mu(T)^2/f$, the mobility-temperature dependence for a dominant scattering mechanism (i.e. APs) can be related to $S_I(f)$. Previous experimental findings demonstrate that similar $\mu - T$ and $S_I(f) - T$ relationships can be used to identify the type of mobility-fluctuations giving rise to 1/*f* noise. For this, we use our model to identify the temperature dependence of $S_I(f)$ dominated by AP/POPs in the 2DEG. We expect $S_I(f) \propto T^{-1}$ with POPs and $S_I(f) \propto T^{-2}$ with APs. Tracking the evolution of *k*-state occupation over time in the linear bias regime [10^5 Vcm^{-1}] at 77 K, 100 K, and 300 K (Fig. 2 (d,e,f)), we observe a subtle trend with increased temperature. At higher temperatures (300 K), the electrons diffuse further away from the path of the applied field compared to lower temperatures due to the increased phonon number ($n_{ph} \propto e^{-1/T}$), leading to more frequent scattering. $S_I(f)$ is extracted from the simulation (Fig. 2(h)) and shows a decrease in noise amplitude with increased temperature, as expected. However, $S_I(f)$ must be simulated over a wider range of temperatures to demonstrate the expected T^{-1} and T^{-2} dependence for POP and AP scattering.

Challenges and opportunities

The development of a characterization technique and microscopic model to measure and predict the 1/*f* noise spectral density of III-V nitride highly degenerate channels presents an important set of tools for identifying the origins of this phenomena and to potentially suppress this behavior which is detrimental in the manifestation of modern electronics. We have shown both experimentally and theoretically that 1/*f* noise is less detrimental to a device's operation at high fields and have demonstrated that the SNR of III-V 2DEG channels is strongly influenced by polar optical phonon and acoustic phonon scattering events. However, both the characterization technique and Monte Carlo model presently demonstrates limitations in identifying the origins of 1/*f* noise in other highly degenerate III-V materials.

Extending our Monte Carlo simulator to one that that captures extrinsic scattering, intervalley scattering, assumes non-parabolic bands, and uses an anisotropic phonon dispersion will lead to an accurate physical insight of the noise physics in III-V devices and will be particularly useful in describing the noise origins in GaN *p*-channel devices.

References

1. Pearson, G. L. *Phys. Rev.* **5**, 233-243 (1934).
2. Pearson, G. L, *The Bell System Technical Journal*, **13**, 634-653 (1934)
3. Van Der Ziel, A., *PRECIEDINGS OF THE IEEE* **76**, 3 (1988).
4. Hooge, F.N., *IEEE TRANSACTIONS ON ELECTRONIC DEVICES.* **41,** 2 (1994).
5. Hooge F.N. *Advanced Experimental Methods for Noise Research in Nanoscale Electronic Devices.* **151** (2004)
6. Vandamme, L. K. J., & Hooge, F. N. (2008). What do we certainly know about 1/f noise in MOSTs? *IEEE Transactions on Electron Devices*. https://doi.org/10.1109/TED.2008.2005167
7. De Graaff, H. C., & Huybers, M. T. M. (1983). 1/f noise in polycrystalline silicon resistors. *Journal of Applied Physics*. https://doi.org/10.1063/1.332369
8. Balandin, A. A. (2013). Low-frequency 1/f noise in graphene devices. *Nature Nanotechnology*. https://doi.org/10.1038/nnano.2013.144
9. Renteria, J., Samnakay, R., Rumyantsev, S. L., Jiang, C., Goli, P., Shur, M. S., & Balandin, A. A. (2014). Low-frequency 1/f noise in MoS2 transistors: Relative contributions of the channel and contacts. *Applied Physics Letters*. https://doi.org/10.1063/1.4871374
10. Fleetwood, D. M., Wang, P., Chen, J., Jiang, R., Zhang, E. X., McCurdy, M. W., & Schrimpf, R. D. (2017). 1/f noise in GaN/AlGaN HEMTs. *2016 13th IEEE International Conference on Solid-State and Integrated Circuit Technology, ICSICT 2016 - Proceedings*. https://doi.org/10.1109/ICSICT.2016.7998835
11. Im, K. S., Choi, J., Hwang, Y., An, S. J., Roh, J. S., Kang, S. H., … Lee, J. H. (2019). 1/f noise characteristics of AlGaN/GaN HEMTs with periodically carbon-doped GaN buffer layer. *Microelectronic Engineering*. https://doi.org/10.1016/j.mee.2019.110985
12. Liu, Y., & Zhuang, Y. (2014). A gate current 1/f noise model for GaN/AlGaN HEMTs. *Journal of Semiconductors*. https://doi.org/10.1088/1674-4926/35/12/124005
13. Balandin, A., Wang, K. L., Cai, S., Li, R., Viswanathan, C. R., Wang, E. N., & Wojtowicz, M. (2000). Investigation of flicker noise and deep-levels in GaN/AlGaN transistors. *Journal of Electronic Materials*. https://doi.org/10.1007/s11664-000-0066-8
14. Rao, H., & Bosman, G. (2009). Simultaneous low-frequency noise characterization of gate and drain currents in AlGaN/GaN high electron mobility transistors. *Journal of Applied Physics*. https://doi.org/10.1063/1.3259437
15. Zhang, A. P., Rowland, L. B., Kaminsky, E. B., Tilak, V., Grande, J. C., Teetsov, J., … Eastman, L. F. (2003). Correlation of device performance and defects in AlGaN/GaN high-electron mobility transistors. *Journal of Electronic Materials*. https://doi.org/10.1007/s11664-003-0163-6
16. Chaudhuri, R., Bader, S. J., Chen, Z., Muller, D. A., Xing, H. G., & Jena, D. (2019). A polarization-induced 2D hole gas in undoped gallium nitride quantum wells. *Science*. https://doi.org/10.1126/science.aau8623
17. Bader, S. J., Chaudhuri, R., Schubert, M. F., Then, H. W., Xing, H. G., & Jena, D. (2019). Wurtzite phonons and the mobility of a GaN/AlN 2D hole gas. *Applied Physics Letters*. https://doi.org/10.1063/1.5099957
18. Mishra, U. K., Parikh, P., & Wu, Y. F. (2002). AlGaN/GaN HEMTs - An overview of device operation and applications. *Proceedings of the IEEE* https://doi.org/10.1109/JPROC.2002.1021567

19. Mizuno, S., Yamada, F., Yamamoto, H., Nishihara, M., Yamamoto, T., & Sano, S. (2012). Development of GaN HEMT for microwave wireless communications. *SEI Technical Review*.
20. Ohno, Y., & Kuzuhara, M. (2001). Application of GaN-based heterojunction FETs for advanced wireless communication. *IEEE Transactions on Electron Devices*. https://doi.org/10.1109/16.906445
21. Khandelwal, S., Goyal, N., & Fjeldly, T. A. (2011). A physics-based analytical model for 2DEG charge density in AlGaN/GaN HEMT devices. *IEEE Transactions on Electron Devices*. https://doi.org/10.1109/TED.2011.2161314
22. Sanabria, C., Xu, H., Palacios, T., Chakraborty, A., Heikman, S., Mishra, U. K., & York, R. A. (2005). Influence of epitaxial structure in the noise figure of AlGaN/GaN HEMTs. *IEEE Transactions on Microwave Theory and Techniques*. https://doi.org/10.1109/TMTT.2004.840578
23. Liu, Y., & Zhuang, Y. (2014). A gate current 1/f noise model for GaN/AlGaN HEMTs. *Journal of Semiconductors*. https://doi.org/10.1088/1674-4926/35/12/124005
24. Fang, T., Konar, A., Xing, H., & Jena, D. (2011). High-field transport in two-dimensional graphene. *Physical Review B - Condensed Matter and Materials Physics*. https://doi.org/10.1103/PhysRevB.84.125450
25. Ramonas, M., Matulionis, A., & Rota, L. (2003). Monte Carlo simulation of hot-phonon and degeneracy effects in the AlGaN/GaN two-dimensional electron gas channel. *Semiconductor Science and Technology*. https://doi.org/10.1088/0268-1242/18/2/310
26. Yu, T. H., & Brennan, K. F. (2002). Monte Carlo calculation of two-dimensional electron dynamics in GaN-AlGaN heterostructures. *Journal of Applied Physics*. https://doi.org/10.1063/1.1448889
27. Bhapkar, U. V., & Shur, M. S. (1997). Monte Carlo calculation of velocity-field characteristics of wurtzite GaN. *Journal of Applied Physics*. https://doi.org/10.1063/1.365963
28. Gökden, S. (2003). Mobility of two-dimensional electrons in an ALGaN/GaN modulation-doped heterostructure. *Physica Status Solidi (A) Applied Research*. https://doi.org/10.1002/pssa.200306701
29. Knap, W., Borovitskaya, E., Shur, M. S., Hsu, L., Walukiewicz, W., Frayssinet, E., … Grzegory, I. (2002). Acoustic phonon scattering of two-dimensional electrons in GaN/AlGaN heterostructures. *Applied Physics Letters*. https://doi.org/10.1063/1.1448401
30. Friedland, K. J., Hey, R., Kostial, H., Klann, R., & Ploog, K. (1996). New concept for the reduction of impurity scattering in remotely doped gaas quantum wells. *Physical Review Letters*. https://doi.org/10.1103/PhysRevLett.77.4616
31. Pokatilov, E. P., Nika, D. L., & Balandin, A. A. (2004). Confined electron-confined phonon scattering rates in wurtzite AlN/GaN/AlN heterostructures. *Journal of Applied Physics*. https://doi.org/10.1063/1.171070

Acknowledgments
We thank Zacharay Boynton, Samuel J. Bader, and Guru Khasla for fruitful discusssions regarding the development of a 1/*f* noise simulator and conducting the measurements. For the measurements performed here, we made use of the Cornell Center for Materials Research (CCMR) and the Cornell NanoScale Science and Technology Facility.

Author information
The authors declare no competing financial interests. Correspondence and request for materials should be adressed to N.L (nl475@cornell.edu) or D.J. (djena@cornell.edu).

Extended methods: Monte Carlo simulator for the prediction of $1/f$ noise in degenerate semiconductors

Nima Leclerc[1*] , Menyoung Lee[2], Reet Chaudhuri[2], Huili Grace Xing[1,2], and Debdeep Jena[1,2]
[1] School of Electrical and Computer Engineering, Cornell University, Ithaca, New York 14853, USA.
[2] Department of Materials Science and Engineering, Cornell University, Ithaca, New York 14853, USA.

May 18, 2020

Monte Carlo algorithm description

In our implementation of $1/f$ noise simulator for degenerate semiconductors aims at predicting the current power spectral density $S_I(f)$ in a channel which we define as the Fourier transform of the the current autocorrelation function $C_I(\tau)$. Computing $C_I(\tau)$ is the main objective of the Monte Carlo implementation. $C_I(\tau)$ is defined as $C_I(\tau) = \langle \delta I(\tau)\delta I(0)\rangle$ for some lag time τ. The current is written in the k-space representation in terms of group velocities and the occupation function: $I = q\sum_{\mathbf{k}} \mathbf{v}_{\mathbf{k},n} f_{\mathbf{k}}$, with $\mathbf{v}_{\mathbf{k},n} = \frac{1}{\hbar}\nabla\epsilon_{\mathbf{k},n}$ (n corr-0esponds to the conduction band in this single-band intravalley scattering picture). The algorithm directly computes $\mathbf{v}_{\mathbf{k},n}(t)$ over the time of the simulation T_{sim} according to a series of drift and diffusion events in k-space.

Algorithm 1: Scattering limited electron transport Monte Carlo model

Input: k-space mesh, energy eigenvalue(s) $\epsilon_{\mathbf{k},n}$ time step δt, number of electrons , temperature T, electric field $\mathbf{E}$, simulation time T_{sim}, scattering events s_i, set of scattering probability matrices $\{\mathcal{P}_i(\mathbf{k}'|\mathbf{k})\}$
Output: List of visited k points during the simulation and associated velocities $\{(\mathbf{k}_i, \mathbf{v}_i)\}$
Sample initial set of N points from specified k mesh at random $\mathbf{k}_0 \in \mathcal{R}^{N\times 3}$
Initialize empty lists for $\{(\mathbf{k}_i, \mathbf{v}_i)\}$, simulation time t_{sim} to 0
n = 0
while $t_{sim} \leq T_{sim}$ **do**
    $n \leftarrow n + 1$
    for $i = 0 \rightarrow$ *N-1* **do**
        $\mathbf{k}_{0,i} \leftarrow \mathbf{k}_{0,i} + \frac{e\delta t}{\hbar}\mathbf{E}$
        Pick scattering event s_j at random (e.g. acoustic, phonons, polar optical phonons, or self-scattering)
        Pick random $\mathbf{k}_i$ from distribution $\mathcal{P}_j(\mathbf{k}'_m|\mathbf{k}_l)$ and compute state occupancy $f(\mathbf{k}_i, T)$
        if $1 - f(\mathbf{k}_i, T) \leq \epsilon$ && *energy is conserved* && *momentum is conserved* **then**
            $\mathbf{k}_{0,i} \leftarrow \mathbf{k}_{0,i} + \mathbf{k}_i$ and compute scattering time $\tau_{\mathbf{0},\mathbf{k}_i,\mathbf{0},\mathbf{k}_{i+1}}$
            $\mathbf{v}_i \leftarrow \mathbf{v}(\mathbf{k}_{0,i})$
        end
        else
            self-scatter from $\mathbf{k}_{0,i}$
        end
    end
    $t_{sim} \leftarrow n\delta t + \sum_i \tau_{\mathbf{0},\mathbf{k}_i,\mathbf{0},\mathbf{k}_{i+1}}$ Append $\{(\mathbf{k}_j, \mathbf{v}_j)\}$ with $\frac{1}{N}\sum_i \mathbf{k}_i$ and $\frac{1}{N}\sum_i \mathbf{v}_i$.
end

Algorithm 1 outlines our implementation of the MC simulator which returns $\{(\mathbf{k}_i, \mathbf{v}_i)\}$, the list of visited k-points during the simulation and associated ensemble carrier velocities over N particles. A time step δt is specified for the drift step and should be significantly smaller than the particle scattering time $\tau_{\mathbf{k},\mathbf{k}'}$. A typical setting for this is 10^{-15} s. The outer loop goes through every time step until the simulation is complete and the inner loop iterates through every electron in the ensemble (typical setting of 10^4 for a degenerate electron system). Over ever iteration, the k-states evolve according drift and diffusion steps. In the drift evolution step (Line 9 of Algorithm 1), the k-state evolves deterministically in the direction of the driven field $\mathbf{E}$ for a time δt. Next, a scattering event is chosen at random due to either acoustic phonon (AP), polar optical phonon (POP), or self scattering.

For each scattering event, there is a corresponding probability matrix $\mathcal{P}_{i,j}(\mathbf{k}'|\mathbf{k}) \in \mathcal{R}^{n,m}$ (n, m as dimensions of the initialized k-mesh) from which the subsequent k-point is determined in the evolution. The form of this distribution for a scatterer n is given by Equation 1.

$$\mathcal{P}^{(n)}_{i,j}(\mathbf{k}'_i|\mathbf{k}_j) = \frac{\tau^{(n),-1}_{\mathbf{k}'_i,\mathbf{k}_j}}{\sum_{i=0}^{m-1}\sum_{j=0}^{n-1}\tau^{(n),-1}_{\mathbf{k}'_i,\mathbf{k}_j}} \tag{1}$$

Here, the scattering rates are determined from Fermi's Golden rule. Under self-scattering, $\mathcal{P}^{(n)}_{i,j}(\mathbf{k}'_i|\mathbf{k}_j) = 0$. For APs and POPs, the expressions are defined in (2).

$$\begin{aligned}\tau^{(n),-1}_{\mathbf{k}'_i,\mathbf{k}_j} = \frac{2\pi}{\hbar}|\langle\psi_{\mathbf{k}_{i+1}}|\hat{W}^{(n)}|\psi_{\mathbf{k}_i}\rangle|^2[n_{\mathbf{q}}\delta_{\mathbf{k}_{i+1}=\mathbf{k}_i+\mathbf{q}}\delta(E_{C,\mathbf{k}_{i+1}} - E_{C,\mathbf{k}_i} - \hbar\omega_{\mathbf{q}}) \\ +(n_{\mathbf{q}}+1)\delta_{\mathbf{k}_{i+1}=\mathbf{k}_i-\mathbf{q}}\delta(E_{C,\mathbf{k}_{i+1}} - E_{C,\mathbf{k}_i} + \hbar\omega_{\mathbf{q}})]\end{aligned} \tag{2}$$

In the above expression$\hat{W}^{(n)}$ is the scattering potential for mechanism n ($n = 1$ for AP and $n = 2$ for POP), $\mathbf{q}$ is the momentum of the phonon used during scattering, and $n_{\mathbf{q}}$ is the phonon number (for a given temperature T and phonon of momentum $\mathbf{q}$). The 2 terms in the expression correspond to phonon adsorption and phonon emission. For $n = 1$, a linear dispersion is assumed for the phonon frequencies ($\hbar\omega_{\mathbf{q}} \sim \mathbf{q}$). For $n = 2$, a dispersion-less phonon band structure is assumed and $\hbar\omega_{\mathbf{q}} \sim 200$meV.

In our implementation, we used Fang-Howard wave functions as ground states for the two-dimensional electron gas (2DEG) which has a parabolic band structure (Equation 4,5). Here, z is the spatial dimension perpendicular to the 2DEG surface, $\mathbf{r}$ is the spatial dimension along the lateral surface, E_C is the conduction band at the Γ-point, b is the variational parameter, and $m^\star_{ij}$ is the effective mass along the ij direction. This electronic states are used to determine analytical forms of the scattering rates above.

$$\psi = \chi_n(z)e^{i\mathbf{k}\cdot\mathbf{r}}, \chi_0(z) = \sqrt{\frac{b^3z^2}{2}}e^{-bz/2} \tag{3}$$

$$E_C(\mathbf{k}) = E_C + \frac{\hbar^2}{2}(\frac{k_x^2}{m^\star_{xx}} + \frac{k_y^2}{m^\star_{yy}}) \tag{4}$$

The algorithm described above gives a time-sequence of k-points and corresponding electron velocities $\{(\mathbf{k}_i, \mathbf{v}_i)\}$ for the ensemble of electrons. If implemented correctly, one should expect a velocity overshoot at the beginning of simulation followed by saturation. The velocity autocorrelation function $C_{\mathbf{v}}(\tau)$ over the time series is determined from the definition in Equation 6 with $\delta\mathbf{v} = \mathbf{v} - \langle\mathbf{v}\rangle$.

$$C_{\mathbf{v}}(\tau) = \langle\delta\mathbf{v}(\tau)\delta\mathbf{v}(0)\rangle \tag{5}$$

The current autocorrelation is obtained from $C_{\mathbf{v}}(\tau)$ as $C_I(\tau) = e^2C_{\mathbf{v}}(\tau)$ with e as electron charge. Computing the fast Fourier transform of $C_I(\tau)$ gives the current noise power spectral density $S_I(f)$, a quantity that can be experimentally measured across a semiconductor channel with a spectrum analyzer.

Code availibility

The open-source code can be found available at `https://github.com/nimalec/monte_carlo_electronic_noise`.